Front. Phys. 10, 101202 (2015)
DOI 10.1007/s11467-015-0471-3

RESEARCH ARTICLE

Electron–positron pair production in the low-density approximation

Nuriman Abdukerim, Zi-Liang Li, Bai-Song Xie†

Key Laboratory of Beam Technology and Materials Modification of the Ministry of Education, and College of Nuclear Science and Technology, Beijing Normal University, Beijing 100875, China

Corresponding author. E-mail: †bsxie@bnu.edu.cn

Received January 26, 2015; accepted March 24, 2015

Electron–positron pair creation is studied in the low-density approximation by solving the quantum Vlasov equation exactly and the mapping equation approximately. The simpler mapping equation is an approximate treatment of the quantum Vlasov equation in which the continuous external field is regarded as a series of delta kicks. Our study indicates that this new treatment is appropriate because the results of the two methods are in good agreement with each other. However, as the period number increases, interference and a complicated structure in the momentum distribution are observed. Furthermore, we also obtain the square power law relation of the number density to the applied electric field strength.

Keywords pair production, quantum Vlasov equation, mapping equation

PACS numbers 12.20.Ds, 11.15.Tk

1 Introduction

In the presence of a strong external background field, the quantum electrodynamics vacuum would decay to electron–positron (e^-e^+) pairs [1–4]. The nonperturbative tunneling process is called the Schwinger mechanism, and in 1951 Schwinger [3] obtained the critical field strength of $E_{cr} = m_e^2c^3/(e\hbar) \sim 1.3 \times 10^{16}$ V/cm, where m_e is the electron mass and e is the elementary unit charge. Reaching E_{cr} at present seems difficult; however, by using focused X-ray free-electron laser (XFEL) facilities one can reach a subcritical field strength $E = 0.01E_{cr}$–$0.1E_{cr}$, so that e^-e^+ pair production may be observed in the near future [5–7].

Many different approaches to obtaining the pair production rate and/or number density have been taken; these include the semiclassical method [8–10], the worldline instanton method [11–13], and the quantum kinetic method [5, 6, 14–17], among others [18–22]. It should be emphasized that, among them, the quantum Vlasov equation (QVE) has an obvious advantage since not only the pair production rate but also momentum distribution information can be obtained.

In our past work [23, 24], through solving the QVE numerically with a Runge–Kutta algorithm, we have obtained some interesting and useful results for the momentum distribution and number density of the created e^-e^+ pairs; these results depend strongly on the shape and parameters of the laser pulsed field. In fact, for weak fields ($E < E_{cr}$), some researcher have pointed out that it is appropriate to use the low-density approximation, i.e., $f(\boldsymbol{p}, t) \ll 1$, where $f(\boldsymbol{p}, t)$ is the momentum distribution of created pairs, which makes the non-Markovian processes become Markovian [25]. Moreover, it is easier to obtain the momentum distribution and the number density in this approximation [26, 27].

In this paper, in the low-density approximation, we develop a new technique, i.e., by solving the mapping equation (ME) instead of the QVE, to treat the pair production. Obviously, the ME is simpler and more efficient to solve numerically compared to the QVE, because the ME is just an algebraic iteration relation whereas the QVE is a typical ordinary differential equation. Fortunately, we can construct the ME successfully as long as we use a series of delta pulsed sequence fields to replace the original continuous field. By solving both the QVE and the ME we calculate the momentum distribution and the number density. Physically, as the period number and field frequency increase, both approaches can produce a complicated momentum distribution structure. The cellular structure also exhibits a strong interference effect. Quan-

titatively, the results obtained from the ME are always larger than those of the QVE; however, qualitatively, the results are in good agreement with each other based on a numerical comparison. Moreover, we also derive a square power law relation between the number density and the field strength in both QVE and ME approaches. Based on the results presented in this paper we conclude that the simpler ME approach is reasonable and useful in the study of pair production, in particular in the low-density approximation.

We use the electron characteristic quantities as normalized units, i.e., length $\lambda_c = \hbar/(m_e c) = 3.862 \times 10^{-13}$ m, momentum $m_e c = 0.511$ MeV/c, and time $\tau_e = \lambda_c/c = 1.288 \times 10^{-21}$ s. In our study some typical parameters are given as laser frequencies $\omega_1 = 0.08$ and $\omega_2 = 0.15$ and pulse length $\tau = 5\pi/\omega_2$, respectively.

2 Theoretical formalism

Using the XFEL facilities, it is possible to generate a field whose strength $E \leqslant 0.1E_{cr}$. We assume an ideal field in which the magnetic field is neglected, the electric field is time dependent but space homogenous, and plasma oscillations and the internal field E_{int} owing to back reaction can be neglected; consequently, the background field becomes

$$\boldsymbol{E}(t) = -\dot{\boldsymbol{A}} = (0, 0, E(t)), \tag{1}$$

where $\boldsymbol{A}$ is the vector potential of the applied field. In the next section we will use three types of fields, E_1, E_2, and E_3. Because the field strength we studied is much smaller than E_{cr} and indeed $f(\boldsymbol{p}, t) \ll 1$ holds, we can use the low-density approximation.

2.1 Quantum Vlasov equation

When the source term $s(\boldsymbol{p}, t)$ depends only on the applied external field as well as the e^-e^+ kinetic property, from $\mathrm{d}f(\boldsymbol{p}, t)/\mathrm{d}t = s(\boldsymbol{p}, t)$ we get the following integro-differential equation describing the time evolution of the pair creation distribution:

$$\frac{\mathrm{d}f(\boldsymbol{p}, t)}{\mathrm{d}t} = \frac{eE(t)\varepsilon_\perp^2}{\omega^2(\boldsymbol{p}, t)} \int_{t_0}^{t} \mathrm{d}t' \frac{eE(t')[1 - f(\boldsymbol{p}, t')]}{\omega^2(\boldsymbol{p}, t')} \cdot \cos\left[2\int_{t'}^{t} \mathrm{d}t'' \omega(\boldsymbol{p}, t'')\right], \tag{2}$$

where $\boldsymbol{p} = (\boldsymbol{p}_t, p_l)$ is the electron/positron canonical three-momentum, $\varepsilon_\perp^2 = m_e^2 + \boldsymbol{p}_t^2$ is the transverse energy squared, $\omega^2(\boldsymbol{p}, t) = \varepsilon_\perp^2 + p_k^2(t)$ is the total energy squared, and $p_k(t) = p_l - eA(t)$ is the kinetic momentum. Note that, if we define $\Theta(\boldsymbol{p}, t', t) = \int_{t'}^{t} \omega(\boldsymbol{p}, t'')\mathrm{d}t''$ and $q(\boldsymbol{p}, t) = eE(t)\varepsilon_\perp^2/\omega^2(\boldsymbol{p}, t)$, then Eq. (2) becomes

$$\frac{\mathrm{d}f(\boldsymbol{p}, t)}{\mathrm{d}t} = q(\boldsymbol{p}, t) \int_{t_0}^{t} \mathrm{d}t' q(\boldsymbol{p}, t')[1 - f(\boldsymbol{p}, t')] \cdot \cos[2\Theta(\boldsymbol{p}, t', t)], \tag{3}$$

where the Pauli-blocking term $[1 - f(\boldsymbol{p}, t)]$, owing to the statistical behaviors of electrons and positrons as fermions, reveals clearly the memory effect that the solution of the differential equation depends on the full time evolution of the distribution function. Certainly, in the low-density limit of $f(\boldsymbol{p}, t) \ll 1$, the Pauli-blocking term becomes $\sim$1 and the memory effect would disappear, so that the system would become a Markovian process [25, 28]. Now Eq. (3) can be written as

$$\frac{\mathrm{d}f(\boldsymbol{p}, t)}{\mathrm{d}t} = q(\boldsymbol{p}, t) \int_{t_0}^{t} \mathrm{d}t' q(\boldsymbol{p}, t') \cos[2\Theta(\boldsymbol{p}, t', t)]. \tag{4}$$

For convenience, we can denote the integral part in Eq. (7) as $g(\boldsymbol{p}, t)$. The equation can then be further expressed as a set of first-order ordinary differential equations (ODEs) [14]:

$$\dot{f}(\boldsymbol{p}, t) = q(\boldsymbol{p}, t) g(\boldsymbol{p}, t), \tag{5}$$

$$\dot{g}(\boldsymbol{p}, t) = q(\boldsymbol{p}, t) - 2\omega(\boldsymbol{p}, t) w(\boldsymbol{p}, t), \tag{6}$$

$$\dot{w}(\boldsymbol{p}, t) = 2\omega(\boldsymbol{p}, t) g(\boldsymbol{p}, t). \tag{7}$$

For simplicity, we have denoted the time derivatives with a dot above the physical quantities.

Obviously, the initial conditions can be given as $f(\boldsymbol{p}, t_0)$, $g(\boldsymbol{p}, t_0)$, and $w(\boldsymbol{p}, t_0)$ in terms of concrete physical problems. Integrating the distribution function to momentum we can get the time-dependent e^-e^+ pair number density

$$n(t) = \int \frac{\mathrm{d}^3 p}{(2\pi)^3} f(\boldsymbol{p}, t), \tag{8}$$

while $f(\boldsymbol{p}, t)$ describes the created real particles only when $t \to +\infty$.

To see the effect of different frequencies and also the effect of the pulse, in our numerical calculation three types of field $E(t)$ are chosen: (i) $E_1 = \varepsilon_0 \sin(\omega_1 t)$, $0 \leqslant t \leqslant NT_1$, where the integer N is the number of periods and $T_1 = 2\pi/\omega_1$ is the period; (ii) $E_2 = \varepsilon_0 \sin(\omega_2 t)$, $0 \leqslant t \leqslant NT_2$, $T_2 = 2\pi/\omega_2$, and (iii) $E_3 = \varepsilon_0 \sin(\omega_2 t)/\cosh^2(t/\tau)$, $-\tau \leqslant t \leqslant \tau$, where τ is the pulse duration.

2.2 Mapping equation

In many physical problems, for example, in the rotor model of nonlinear dynamics and atomic ionization and stabilization in strong fields, for convenience of numerical calculations, the simple mapping equation can be used

instead of the original complicated differential equation. Certainly, the validity of the ME depends on the concrete physical problem. In general, for a relatively fast varying field this approximation is more reasonable. However, still lacking is a rigorous criterion for its validity except for the reliability of results compared to the accurate ones. The advantage of using the ME is not only the simplicity of the treatment but also its ability to distinguish the main physical characteristics.

For simplicity in this paper, we regard the field as a superposition of a series of delta type pulse functions, for example, $E_1(t) = \sum_{i=1}^{I} \varepsilon_0 \sin(\omega_1 t)\delta(t-i) = \sum_{i=1}^{I} E_1(i)\delta(t-i)$, where $1 \leqslant i \leqslant I$ with $I = N[T]$ (where i and I are integers and [ ] indicates a function giving the maximum integer that is smaller than or equal to the variable), and $E_1(i) = \varepsilon_0 \sin(\omega_1 i)$. Similarly one has $E_2(t) = \sum_{i=1}^{I} E_2(i)\delta(t-i)$ and $E_3(t) = \sum_{i=1}^{I} E_3(i)\delta(t-i)$ with $E_2(i) = \varepsilon_0 \sin(\omega_2 i)$ and $E_3(i) = \varepsilon_0 \sin(\omega_2 i)/\cosh^2(i/\tau)$, respectively.

In the low-density approximation, the corresponding ME can be conveniently obtained from Eq. (3) as

$$f_p(i) = f_p(i-1) + q_p(i)\sum_{j=1}^{i}\{q_p(j)\cos[2\Theta(j,i)]\}, \quad (9)$$

where $q_p(i) = eE(i)\varepsilon_\perp/\omega_p^2(i)$, $\Theta(j,i) = \sum_{k=j}^{i}\omega_p(k)$, $\omega_p(j) = \sqrt{\varepsilon_\perp^2 + [p_l - eA(j)]^2}$, and $A(j) = -\sum_{k=1}^{i} E(k)$. Here j and k are integers and $1 \leqslant j \leqslant i \leqslant I$.

3 Numerical results and discussion

In this section, the e^-e^+ momentum distribution and number density are obtained by solving the QVE and the ME. The numerical results of the two approaches are compared and a square power law is obtained for the number density dependence of the external field strength.

The dependence of the momentum distribution on the longitudinal momentum at $\boldsymbol{p}_t = 0$ is depicted in Fig. 1 when $E = E_1$ and $N = 1$. The QVE and ME results are plotted in Figs. 1(a) and (b), respectively. One can see that the numerical results for this momentum distribution obtained with the two approaches are almost the same qualitatively but that, quantitatively, the ME results are a little larger than those of the QVE. For example, the maximum value of f in the ME is overestimated by ∼18.9% compared to that of the QVE. We suspect that the ME results are always a little larger than those of the QVE because the delta kick used in the ME greatly increases the instantaneous field. However, the superposition of different delta kicks indicates that more different fields with different frequencies take part in the pair production compared to the QVE case in which fields with fewer frequencies contribute. As our previous studies [29] have shown, the use of multiple fields with multiple frequencies would improve the pair creation rate.

The dependence of the momentum distribution on the full momentum is also plotted in contours in Fig. 2 for $E = E_1$. The results for $N = 1$ and $N = 4$ are shown in the upper [(a) and (b)] and in lower [(c) and (d)] panels, respectively. The QVE and ME results are plotted in (a) and (c) and in (b) and (d), respectively. From this figure it is seen that the momentum distribution exhibits interference to some extent. It is well known that the interference effect comes from the coupling of the transverse and longitudinal momenta. In the lower panel, the momentum distribution becomes more complicated, the interference effect becomes stronger, and the maximum value of f is larger than that in the upper panel. These attributes are associated with the larger period number. Similarly, the ME values are larger than those of the QVE; for example, in the upper and lower panels, the maximal values of f in the ME are overestimated by ∼18.9% and ∼59.3% compared to those in the QVE, respectively.

When the field is chosen as $E = E_2$, the dependence

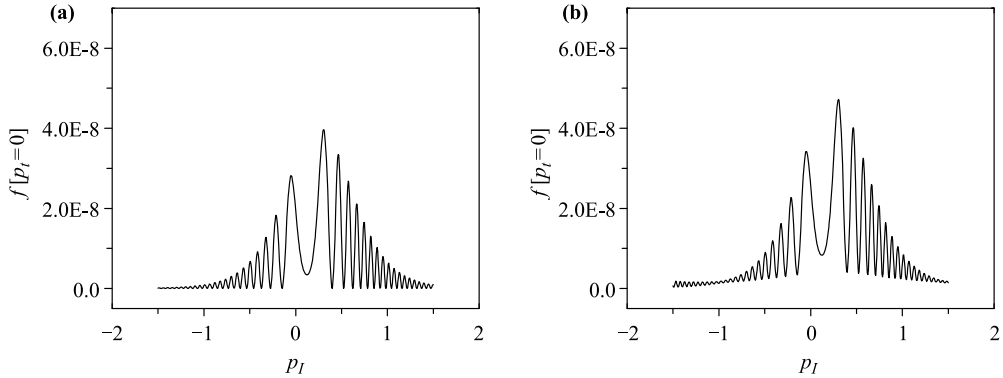

Fig. 1 Momentum dependence of the distribution function for field E_1 when $\boldsymbol{p}_t = 0$, $\omega_1 = 0.08$, $\varepsilon_0 = 0.01$, and $N = 1$ in the case of **(a)** the QVE and **(b)** the ME.

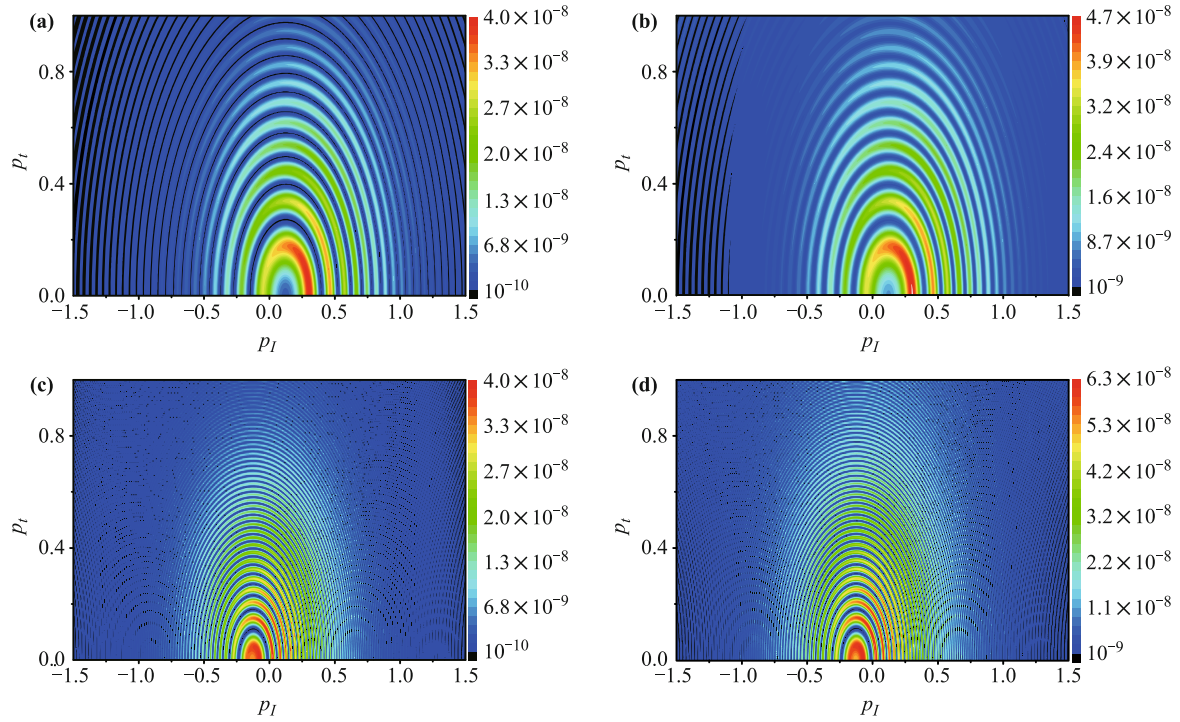

Fig. 2 Contour plots of the momentum distribution for field E_1 in full momentum space when $\omega_1 = 0.08$ and $\varepsilon_0 = 0.01$. The upper and lower panels are for $N = 1$ and $N = 4$, respectively, and the left [**(a, c)**] and right [**(b, d)**] panels are the QVE and ME results, respectively.

of the momentum distribution on the full momentum is plotted in Fig. 3, where the upper and lower panels show the results for $N = 1$ and $N = 10$, respectively. By comparing the upper panel in Fig. 2 with that in Fig. 3, one can observe that the maximum value of f in Fig. 3 is larger than that in Fig. 2 because the field frequency is increasing. In the lower panel of Fig. 3, because of the increase in both the field frequency and the field period number, the momentum distribution appears to have a more complicated cellular structure, which increases the value of f. This structure can be understood from the viewpoint of the semiclassical analytical method [17]. We know that the greater the number of turning points, those points that satisfy the equation $\omega^2(\boldsymbol{p}, t) = 0$ in the upper half of the complex t plane, the more complicated the momentum distribution structure appears. This would generate strong interference, and, as a result, the number density would be enhanced. From both Figs. 2 and 3, although there are some numerical differences between the QVE and ME results, we observe that the resulting pattern structures of the momentum distribution are in good agreement with each other.

Finally, the dependence of the pair number density n on the field strength ε_0 is depicted in Fig. 4 when ε_0 changes from 0.001 to 0.012 for fields E_2 (upper panel) and E_3 (lower panel). The results of $\boldsymbol{p}_t = 0$ are plotted in panels (a) and (c) and that of full momentum are plotted in panels (b) and (d). The QVE and ME results are shown by the black circle and triangle symbols, respectively. The red dashed lines and the dotted lines are their respective linear fittings.

First, from Fig. 4 one can see that the values in panel (a) [or (c)] are larger than those of panel (b) [or (d)]. This is because, near the point $\boldsymbol{p}_t = 0$, the value of f reaches its maximum $f(p_l, p_t = 0, t)$; however, at the other points, the value of f decreases gradually. When $\boldsymbol{p}_t = 0$, the number density is just the integration of $f(p_l, p_t = 0, t)$ along the longitudinal momentum and the transverse contribution can be regarded as 1 so that the values obtained by integrating the momentum distribution only in the longitudinal momentum are larger than those in the full momentum. Second, the pair number densities created in E_3 (lower panel) are smaller than those in E_2 (upper panel). This is because the superposition of a Sauter-type field leads to damping of the oscillation structure. As a result, the number density decreases. Third, in Fig. 4 the values of n in the ME are still larger than those in the QVE. For example, in (b), when $\varepsilon_0 = 10^{-3}$, we have $n_{\mathrm{QVE}} = 4.80 \times 10^{-12}$ and $n_{\mathrm{ME}} = 1.88 \times 10^{-11}$. In this case, the value of n in the ME is overestimated by a factor of $\sim$3 compared to that in the QVE. Last, it is very interesting that both the QVE and the ME exhibit the same power law for the relation between number density n and field strength ε_0

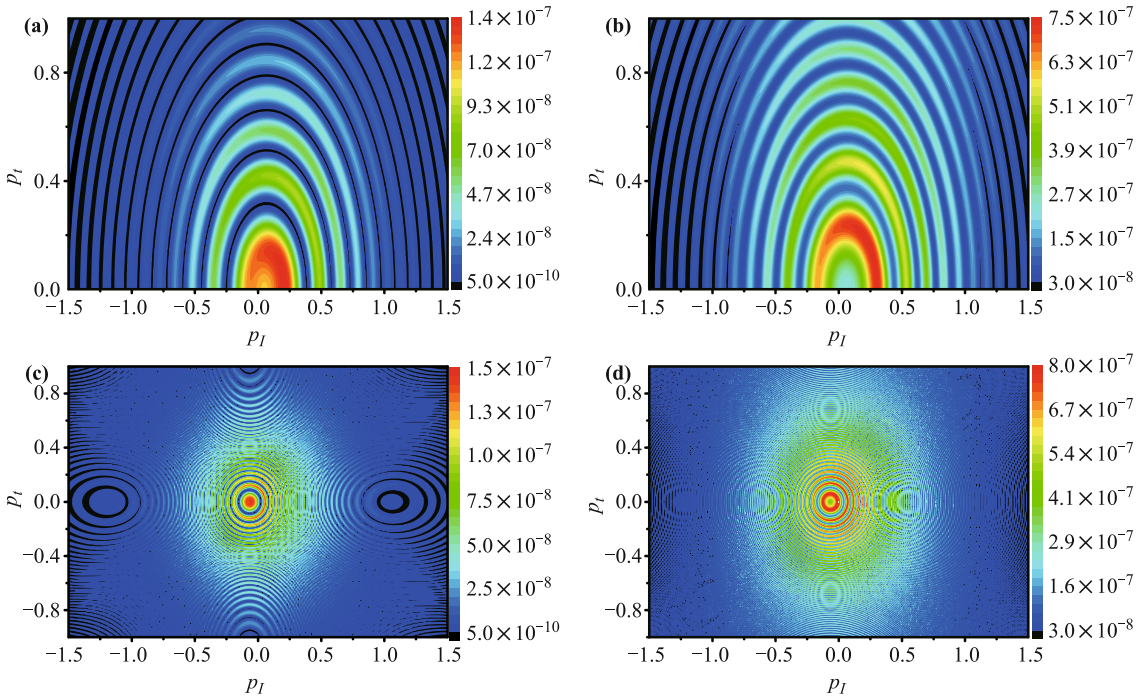

Fig. 3 Contour plots of the momentum distribution for field E_2 in full momentum space when $\omega_2 = 0.15$ and $\varepsilon_0 = 0.01$. The upper and lower panels are for $N = 1$ and $N = 10$, respectively, and the left [**(a, c)**] and right [**(b, d)**] panels are the QVE and ME results, respectively.

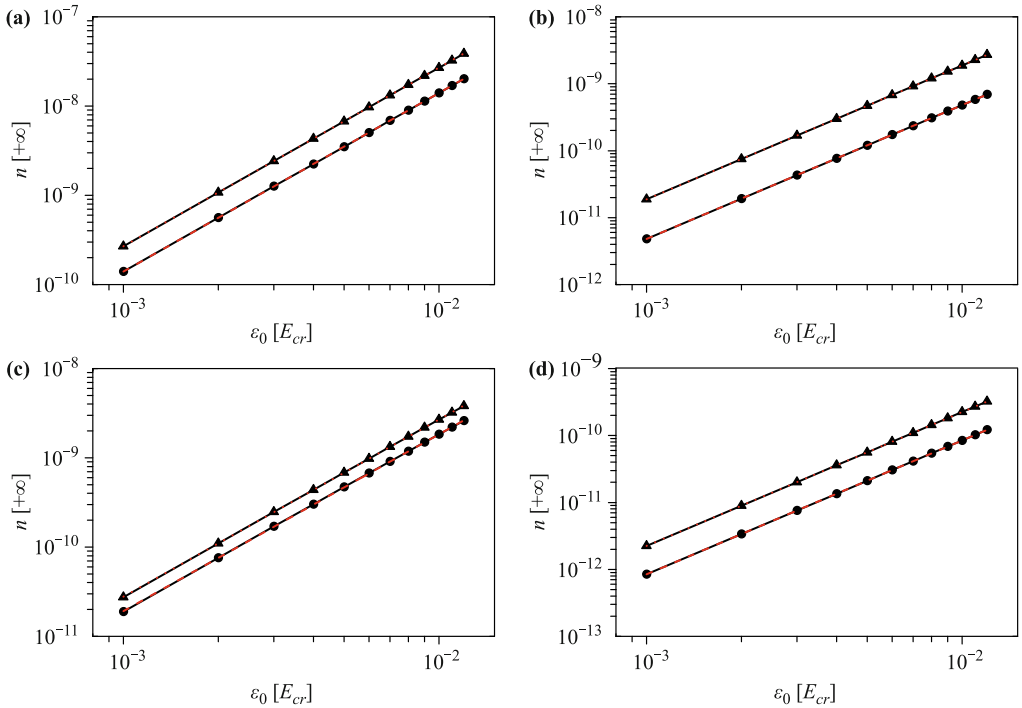

Fig. 4 Number density versus field strength ε_0 in the range $\varepsilon_0 = 0.001 - 0.012$. The upper panel is for E_2 and the lower panel is for E_3 with $\tau = 5\pi/\omega_2$. The $\boldsymbol{p}_t = 0$ results are plotted in **(a)** and **(c)** and those of full momentum space are plotted in **(b)** and **(d)**. The QVE and ME results are shown by the black circle and black triangle symbol, respectively.

as

$$n \propto \varepsilon_0^2. \tag{10}$$

Even the numerical fitting error is kept within 1% for this square law.

4 Conclusions

In this paper, we propose an approximate mapping approach to study pair production in the low-density approximation. By solving the QVE and the ME e^-e^+ pair production in a sine-type and Sauter-type pulsed electric field is studied. For different period number and field frequency, the dependence of the momentum distribution on momentum and the dependence of the number density on field strength are obtained. Increasing field strength and period number lead to complication of the momentum distribution structure. Because more turning points appear, the interference effect becomes stronger, enhancing the number density. In the low-density approximation our studies have shown that the QVE and ME results are in good agreement with each other qualitatively while the latter always gives larger values but within the same order of magnitude. Considering the simplicity and numerical calculation time, we conclude that using the ME is a proper choice. Finally, both the QVE and the ME give the same square power law for the dependence of number density on the field strength when the field strength lies far below the subcritical one.

Acknowledgements This work was supported by the National Natural Science Foundation of China (NSFC) (Grant Nos. 11475026, 11175023, and 11335013), and was also partially supported by the Open Fund of the National Laboratory of Science and Technology on Computational Physics at IAPCM, and the Fundamental Research Funds for the Central Universities (FRFCU).

References

1. F. Sauter, Uber das Verhalten eines Elektrons im homogenen elektrischen Feld nach der relativistischen Theorie Diracs, *Z. Phys.* 69(11–12), 742 (1931)
2. W. Heisenberg and H. Euler, Folgerungen aus der Diracschen Theorie des Positrons, *Z. Phys.* 98(11–12), 714 (1936)
3. J. S. Schwinger, On Gauge invariance and vacuum polarization, *Phys. Rev.* 82(5), 664 (1951)
4. E. Brezin and C. Itzykson, Pair production in vacuum by an alternating field, *Phys. Rev. D* 2(7), 1191 (1970)
5. R. Alkofer, M. B. Hecht, C. D. Roberts, S. M. Schmidt, and D. V. Vinnik, Pair creation and an X-ray free electron laser, *Phys. Rev. Lett.* 87(19), 193902 (2001)
6. C. D. Roberts, S. M. Schmidt, and D. V. Vinnik, Quantum effects with an X-ray free-electron laser, *Phys. Rev. Lett.* 89(15), 153901 (2002)
7. A. Ringwald, Pair production from vacuum at the focus of an X-ray free electron laser, *Phys. Lett. B* 510(1–4), 107 (2001)
8. V. S. Popov, Pair production in a variable external field (Quasiclassical approximation), *Sov. Phys. JETP* 34, 709 (1972)
9. M. S. Marinov and V. S. Popov, Electron–positron pair creation from vacuum induced by variable electric field, *Fortschr. Phys.* 25(1–12), 373 (1977)
10. S. S. Bulanov, Pair production by a circularly polarized electromagnetic wave in a plasma, *Phys. Rev. E* 69(3), 036408 (2004)
11. G. V. Dunne and Q. H. Wang, Multidimensional worldline instantons, *Phys. Rev. D* 74(6), 065015 (2006)
12. R. Schützhold, H. Gies, and G. V. Dunne, Dynamically assisted Schwinger mechanism, *Phys. Rev. Lett.* 101(13), 130404 (2008)
13. B. S. Xie, M. Melike, and D. Sayipjamal, Electron–positron pair production in an elliptic polarized time varying field, *Chin. Phys. Lett.* 29(2), 021102 (2012)
14. F. Hebenstreit, R. Alkofer, G. V. Dunne, and H. Gies, Momentum signature for Schwinger pair production in short laser pulses with a subcycle structure, *Phys. Rev. Lett.* 102(15), 150404 (2009)
15. F. Hebenstreit, R. Alkofer, and H. Gies, Schwinger pair production in space- and time-dependent electric fields: Relating the Wigner formalism to quantum kinetic theory, *Phys. Rev. D* 82(10), 105026 (2010)
16. O. Oluk, B. S. Xie, M. A. Bake, and S. Dulat, Electron–positron pair production in a strong asymmetric laser electric field, *Front. Phys.* 9(2), 157 (2014)
17. Z. L. Li, D. Lu, and B. S. Xie, Dynamically assisted pair production for scalar QED by two fields, *Front. Phys.* 10(1), 101201 (2015)
18. T. Heinzl, A. Ilderton, and M. Marklund, Finite size effects in simulated laser pair production, *Phys. Lett. B* 692(4), 250 (2010)
19. M. Orthaber, F. Hebenstreit, and R. Alkofer, Momentum spectra for dynamically assisted Schwinger pair production, *Phys. Lett. B* 698(1), 80 (2011)
20. C. Fey and R. Schützhold, Momentum dependence in the dynamically assisted Sauter–Schwinger effect, *Phys. Rev. D* 85(2), 025004 (2012)
21. Z. L. Li, D. Lu, and B. S. Xie, Multi-slit interference effect in the time domain for boson pair production, *Phys. Rev. D* 89(6), 067701 (2014)
22. E. Akkermans and G. V. Dunne, Ramsey fringes and time-domain multiple-slit interference from vacuum, *Phys. Rev. Lett.* 108(3), 030401 (2012)
23. A. Nuriman, B. S. Xie, Z. L. Li, and D. Sayipjamal, Enhanced electron-positron pair creation by dynamically assisted combinational fields, *Phys. Lett. B* 717(4–5), 465 (2012)

24. N. Abdukerim, Z. L. Li, and B. S. Xie, Effects of laser pulse shape and carrier envelope phase on pair production, *Phys. Lett. B* 726(4–5), 820 (2013)
25. S. Schmidt, D. B. Blaschke, G. Ropke, A. V. Prozorkevich, S. A. Smolyansky, and V. D. Toneev, Non-Makrovian effects in strong-field pair creation, *Phys. Rev. D* 59(9), 094005 (1999)
26. D. B. Blaschke, B. Kampfer, A. D. Panferov, A. V. Prozorkevich, and S. A. Smolyansky, Infulence of laser pulse parameters on the properties of e^-e^+ palsmas created from vacuum, *Contrib. Plasma Phys.* 53(2), 165 (2013)
27. D. B. Blaschke, B. Kämpfer, S. M. Schmidt, A. D. Panferov, A. V. Prozorkevich, and S. A. Smolyansky, Properties of the electron–positron plasma created from a vacuum in a strong laser field: Quasiparticle excitations, *Phys. Rev. D* 88(4), 045017 (2013)
28. Y. Kluger, E. Mottola, and J. M. Eisenberg, Quantum Vlasov equation and its Markov limit, *Phys. Rev. D* 58(12), 125015 (1998)
29. Z. L. Li, D. Lu, B. S. Xie, L. B. Fu, J. Liu, and B. F. Shen, Enhanced pair production in strong fields by multiple-slit interference effect with dynamically assisted Schwinger mechanism, *Phys. Rev. D* 89(9), 093011 (2014)